Statistical Shape Model for Simulation of Realistic Endometrial Tissue

Sebastian Kurtek[1], Chafik Samir[2] and Lemlih Ouchchane[2,3]
[1]*Department of Statistics, The Ohio State University, Columbus, OH, U.S.A.*
[2]*Image Science for Interventional Techniques, UMR CNRS UdA 6284, Auvergne University, Clermont-Ferrand, France*
[3]*Department of Biostatistics, Medical Informatics and Communication Technologies, Clermont University Hospital, Clermont-Ferrand, France*

Keywords: Realistic Simulation, Statistical Modeling, Geodesics, Elastic Deformation, Generalized Cylinders, Re-parametrization, Shape Analysis, Endometriosis, Karcher Mean.

Abstract: We propose a new framework for developing statistical shape models of endometrial tissues from real clinical data. Endometrial tissues naturally form cylindrical surfaces, and thus, we adopt, with modification, a recent Riemannian framework for statistical shape analysis of parameterized surfaces. This methodology is based on a representation of surfaces termed square-root normal fields (SRNFs), which enables invariance to all shape preserving transformations including translation, scale, rotation, and re-parameterization. We extend this framework by computing parametrization-invariant statistical summaries of endometrial tissue shapes, and random sampling from learned generative models. Such models are very useful for medical practitioners during different tasks such as diagnosing or monitoring endometriosis. Furthermore, real data in medical applications in general (and in particular in this application) is often scarce, and thus the generated random samples are a key step for evaluating segmentation and registration approaches. Moreover, this study allows us to efficiently construct a large set of realistic samples that can open new avenues for diagnosing and monitoring complex diseases when using automatic techniques from computer vision, machine learning, etc.

1 INTRODUCTION

Shape is an important feature of an anatomical object. Thus, statistical shape models play a very important role in characterizing and monitoring anatomical structures. Most anatomical objects are three-dimensional and thus their boundaries form surfaces. In this paper, we are focused on shape models of endometrial tissue, which can be represented using cylindrical surfaces. For this purpose we utilize a comprehensive Riemannian framework based on square-root normal fields that allows registration, comparison, deformation, averaging, and modeling of observed shapes. Furthermore, the developed statistical models are useful in subsequent tasks such as simulation of realistic endometrial tissue shapes for registration approaches (Yavariabdi et al., 2013).

Endometriosis is a complex gynecological disease in which endometrial cells (glands and stroma) appear outside their usual locations in the uterine cavity (Brosens et al., 2004). The main symptoms of endometriosis may depend on the site of active endometriosis and are influenced by hormonal changes. This disease affects approximately 10% of women in the reproductive age group and may cause chronic pelvic pain, severe dysmenorrhea, and several digestive problems including diarrhea, occasional constipation, rectal bleeding and infertility. Endometriosis can be found in the pelvic cavity region, specifically in the pelvic peritoneum and pelvic organs. Currently there is no ethiologic cure for endometriosis, but it can be treated in a variety of ways, including using pain medication, hormonal treatments, and laparoscopic surgery in severe cases. An accurate diagnosis must be made in order to obtain important medical information. A key step in the diagnostic process is to develop a statistical model of the shape of the endometrial tissue coming from various imaging modalities in order to evaluate segmentation and registration methods. In this paper, we consider endometrial tissues imaged using magnetic resonance imaging (MRI). Such models provide information about the observed variability in disease groups. Furthermore, due to data scarcity, these models can be used for extensive simulation studies, where valid realizations of diseased endometrial tissues are randomly generated.

While in this paper we only consider modeling

Kurtek S., Samir C. and Ouchchane L..
Statistical Shape Model for Simulation of Realistic Endometrial Tissue.
DOI: 10.5220/0004821904210428
In *Proceedings of the 3rd International Conference on Pattern Recognition Applications and Methods* (ICPRAM-2014), pages 421-428
ISBN: 978-989-758-018-5

endometrial tissue surfaces, the general method described here has many other applications. In medical imaging, researchers are often interested in modeling various anatomies, including subcortical structures in the brain. Studying shapes of 3D structures in the brain is of particular interest because many diseases can potentially be linked to altering these shapes, in conjunction with other physiological symptoms. Thus, shape analysis based on imaging data offers objective and quantitative means to aid in classification and monitoring of different disease types. Other possible applications of shape analysis of 3D objects include facial recognition, body shape analysis, graphics, and many more.

1.1 Related Methods

Researchers have proposed numerous representations of surfaces for the purpose of shape modeling. Several groups have proposed to study shapes of surfaces by embedding them in volumes and deforming the volumes (Grenander and Miller, 1998; Joshi et al., 1997). Such methods are typically computationally expensive because of the high dimensionality of the resulting objects that are analyzed. An alternative approach is based on manually-generated landmarks also termed Kendall's shape analysis (Dryden and Mardia, 1998). While this is a very popular approach in many applications, it requires a set of registered landmarks to represent the surface, which are difficult to obtain in practice. Others have studied 3D shape variabilities using level sets (Malladi et al., 1996), curvature flows (Gu et al., 2007), medial axes (Bouix et al., 2001; Gorczowski et al., 2010), or point clouds via the iterative closest point algorithm (Almhdie et al., 2007).

However, the most natural representation for studying shapes of 3D anatomical objects seems to be using their boundaries, which form parameterized surfaces. Such a representation poses an additional issue of handling the parameterization variability. Some methods (Brechbühler et al., 1995; Styner et al., 2006) tackle this problem by choosing a fixed parameterization, similar to arc-length in the case of parameterized curves. A large set of papers in the literature treat the re-parameterization (or registration) and analysis steps as separate (Cates et al., 2006; Davies et al., 2010). Because in these approaches the two steps are unrelated, the computed registrations tend to be suboptimal and defining proper parameterization-invariant geodesic distances (and statistics) between surfaces is not possible. In a series of papers, Kurtek et al. (Kurtek et al., 2010; Kurtek et al., 2011b; Kurtek et al., 2012; Kurtek et al., 2011a) presented a comprehensive framework for parameterization-invariant shape modeling of surfaces based on the q-map representation. A major drawback of this method is in the definition of the Riemannian metric, which does not have a clear interpretation in terms of the amount of stretching and bending needed to deform one surface into another. This issue was addressed by Jermyn et al. (Jermyn et al., 2012) using a novel representation of surfaces termed square-root normal fields. We adopt their representation in this paper and use it to develop statistical shape models of endometrial tissue surfaces. Our main contribution is in using this methodology to define and compute statistics such as the mean and covariance of endometrial tissues. We utilize these statistics in specifying generative models of endometrial tissue shape and provide a recipe for random sampling from these models.

1.2 Data Description

The data analyzed in this paper are ten endometrial tissue surfaces coming from MRI images. These surfaces are naturally cylindrical, which motivates our statistical model of surfaces with a cylinder parameterization. Figure 1 displays all surfaces in our data set. Note that there is a lot of variation in this data, and thus, parsimonious shape models are very important in this application. We are able to achieve a natural shape model through elastic shape analysis of surfaces. This methodology uses a special Riemannian metric to perform surface registration by achieving invariance to re-parameterizations of surfaces.

2 MATHEMATICAL FRAMEWORK

Let $\mathcal{F}$ be the space of all smooth embeddings of a cylinder in $\mathbb{R}^3$ and let Γ be the set of all boundary-preserving diffeomorphisms from $\mathbb{S}^1 \times [0,1]$ to itself. For a cylindrical surface representing endometrial tissue $f \in \mathcal{F}$, $f \circ \gamma$ represents a re-parameterization of this surface. Since $\mathcal{F}$ is a vector space, the tangent space at $f \in \mathcal{F}$, $T_f(\mathcal{F})$ is $\mathcal{F}$ itself. Using two tangent vectors $v_1, v_2 \in T_f(\mathcal{F})$ one can define the standard inner product on $\mathcal{F}$ and measure distances between surfaces using the $\mathbb{L}^2$ norm. While intuitive, this framework is inappropriate for statistical shape analysis of parameterized surfaces (Jermyn et al., 2012; Kurtek et al., 2010; Kurtek et al., 2011b; Kurtek et al., 2012). Thus, in this work, we will utilize the square-root normal field representation of cylindrical surfaces to perform the statistical analysis. This representation of surfaces (along with the corresponding Riemannian

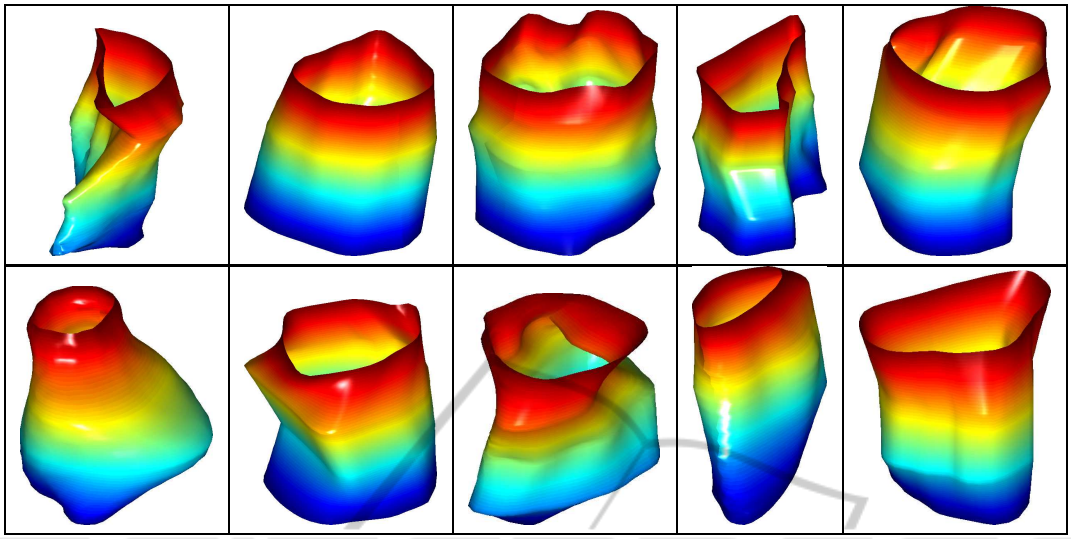

Figure 1: Data set of ten endometrial tissue surfaces coming from MRIs.

metric) were proposed by Jermyn et al. (Jermyn et al., 2012). In the next sections, we provide some mathematical details as well as an algorithm to compute geodesic paths and distances between endometrial tissue surfaces.

2.1 Representation and Registration of Endometrial Tissue Surfaces

Let $n(s) = \frac{\partial f}{\partial u}(s) \times \frac{\partial f}{\partial v}(s) \in \mathbb{R}^3$ denote the normal vector to the endometrial tissue surface at the point $s = (u,v) \in \mathbb{S}^1 \times [0,1]$. Using $n(s)$, Jermyn et al. (Jermyn et al., 2012) defined a mathematical representation of surfaces termed square-root normal fields (SRNFs) as $q(s) = \frac{n(s)}{\sqrt{|n(s)|}}$, where $|\cdot|$ denotes the Euclidean norm in $\mathbb{R}^3$. The space of all SRNFs is a subset of $\mathbb{L}^2(\mathbb{S}^1 \times [0,1], \mathbb{R}^3)$ hereinafter referred to as $\mathbb{L}^2$. We are interested in statistical models of *shapes* of endometrial tissue surfaces. Thus, we must ensure invariance to shape preserving transformations including translation, scale, rotation and re-parameterization. First, note that the SRNF representation is automatically translation invariant. We can achieve scale invariance by re-scaling all surfaces to have unit area. Furthermore, for $O \in SO(3)$ and $f \in \mathcal{F}$, the SRNF of a rotated surface Of is Oq. Also, for $\gamma \in \Gamma$ and $f \in \mathcal{F}$, the SRNF of a re-parameterized surface $f \circ \gamma$ is $(q,\gamma) = (q \circ \gamma)\sqrt{J_\gamma}$, where J_γ is the determinant of the Jacobian of γ. An important property of SRNFs is that if we rotate and re-parametrize any two surfaces in the same way, the $\mathbb{L}^2$-norm between their SRNFs remains unchanged: $\|q_1 - q_2\| = \|(Oq_1,\gamma) - (Oq_2,\gamma)\|$. *This property is necessary to define a shape distance between surfaces, which we later use for subsequent statistical analysis.*

In order to register endometrial tissue surfaces with respect to rotation and parameterization, we first define an equivalence class of an SRNF as $[q] = \{(Oq,\gamma) | O \in SO(3),\ \gamma \in \Gamma\}$. Note that each equivalence class represents a shape of an endometrial tissue surface uniquely. Then, the registration problem can be stated as follows:

$$(O^*,\gamma^*) = \underset{(O,\gamma) \in SO(3) \times \Gamma}{\operatorname{arginf}} \|q_1 - (Oq_2,\gamma)\|^2. \quad (1)$$

This optimization problem is solved iteratively. First, one fixes γ and searches for an optimal rotation over $SO(3)$ using Procrustes analysis. Then, given this rotation, one searches for an optimal re-parameterization over Γ using a gradient descent algorithm presented in (Jermyn et al., 2012) and particularized for use with cylindrical surfaces. In the following sections, we will let $f_2^* = O^*(f_2 \circ \gamma^*)$.

2.2 Geodesics between Endometrial Tissue Surfaces

After optimally registering the endometrial tissue surfaces, we are interested in comparing them using geodesic paths and distances. For this purpose, we utilize a numerical technique termed path-straightening directly on $\mathcal{F}$. This technique was used for computing geodesics between spherical surfaces under a different representation in (Kurtek et al., 2012). It was also specified for the SRNF representation and used in a similar fashion in the application to analysis of cylindrical surfaces. Mainly, we use the geodesics in the definition of the mean and covariance

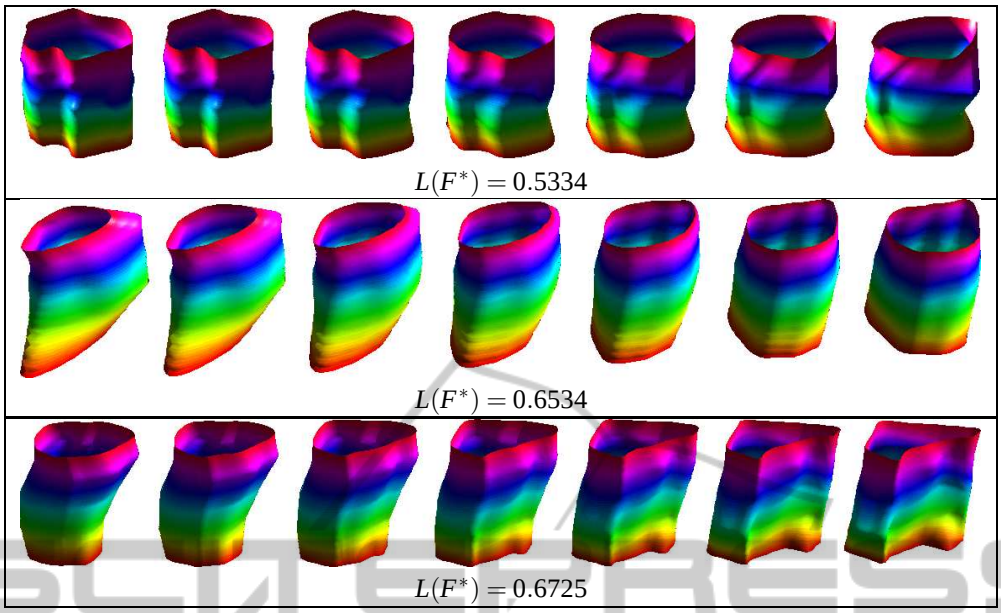

Figure 2: Three examples of geodesic paths between endometrial tissue surfaces and the corresponding geodesic distances.

of endometrial tissue surfaces. Thus, we present a few details next.

We define a Riemannian metric on $\mathcal{F}$ for $w_1, w_2 \in T_f(\mathcal{F})$ as follows:

$$\begin{aligned} & \langle\langle w_1, w_2 \rangle\rangle_f \\ = & \int_{\mathbb{S}^1 \times [0,1]} \frac{(n_{w_1}(s) \cdot n_{w_2}(s))}{|n(s)|} ds \\ - & \frac{3}{4} \int_{\mathbb{S}^1 \times [0,1]} \frac{(n(s) \cdot n_{w_1}(s))(n(s) \cdot n_{w_2}(s))}{|n(s)|^3} ds, \end{aligned}$$

where $n_w(s) = \frac{\partial f}{\partial u}(s) \times \frac{\partial w}{\partial v}(s) + \frac{\partial w}{\partial u}(s) \times \frac{\partial f}{\partial v}(s)$. This metric is the pullback metric of the $\mathbb{L}^2$ metric from the space of SRNFs. In order to compute a geodesic path between two optimally registered endometrial tissue surfaces $f_1, f_2^* \in \mathcal{F}$, we begin by defining the length of a path given by $F : [0,1] \to \mathcal{F}$, $F(0) = f_1$, $F(1) = f_2^*$ using the defined metric (all arguments have been suppressed for brevity):

$$\begin{aligned} & L(F) = \int_0^1 \sqrt{\langle\langle F_t, F_t \rangle\rangle_F} dt \\ = & \int_0^1 \sqrt{\int_{[0,1] \times \mathbb{S}^1} \left[\frac{-3(N \cdot N_t)^2}{4|N|^3} + \frac{|N_t|^2}{|N|} \right] ds dt}. \end{aligned}$$

In the above expression, we use $N(t)$ to represent $\frac{\partial F(t)}{\partial u}(s) \times \frac{\partial F(t)}{\partial v}(s)$ and we denote partial derivatives along the t dimension using subscripts. It is a well known result that a critical point of this path length energy provides a geodesic between f_1 and f_2^* in $\mathcal{F}$. Thus, a geodesic path between two surfaces f_1 and f_2^* is the solution to the following minimization problem:

$$F^* = \underset{F:[0,1] \to \mathcal{F},\, F(0)=f_1,\, F(1)=f_2^*}{\operatorname{argmin}} L(F). \qquad (2)$$

The solution to this problem is computed using a gradient descent approach by approximating ∇L with directional derivatives.

In Figure 2, we present three examples of geodesic paths between registered endometrial tissue surfaces. In addition, we provide the resulting geodesic distance, which is useful in quantifying their shape differences. We note that due to good registration of features, the resulting geodesic paths represent natural deformations between endometrial tissue shapes. This property will also lead to natural summary statistics and shape models, which we consider in the next section.

3 SHAPE STATISTICS OF ENDOMETRIAL TISSUE SURFACES

In this section we present tools and results for computing two fundamental shape statistics, the Karcher mean and the covariance, for a set of cylindrical surfaces. We then utilize these quantities to estimate a generative Gaussian model and draw random samples.

3.1 Estimation of the Karcher Mean

We begin by defining an intrinsic mean shape under the proposed metric, called the Karcher mean. Let $\{f_1, f_2, \ldots, f_n\} \in \mathcal{F}$ denote a sample of endometrial tissue surfaces. Also, let F_i^* denote a geodesic path between a surface f and a surface f_i^* that was optimally registered to f. Then, the sample Karcher mean is given by $\bar{f} = \text{argmin}_{f \in \mathcal{F}} \sum_{i=1}^{n} L(F_i^*)^2$. A gradient-based approach for finding the Karcher mean is given in (Dryden and Mardia, 1998) and is repeated here for convenience. Note that the resulting Karcher mean is a particular element of an equivalence class of surfaces, because our distance (length of the geodesic) is invariant to rotation and re-parameterization.

Algorithm 1: (Karcher Mean). Let $\bar{f}_0$ be an initial estimate of the Karcher mean. Set $j = 0$ and ε_1, ε_2 to be small positive values.
(1) For each $i = 1, \ldots, n$, register f_i to $\bar{f}_j$ using Equation 1 to obtain f_i^*.
(2) For each $i = 1, \ldots, n$, compute the geodesic path between f_i^* and $\bar{f}_j$ using Equation 2.2 to obtain F_i^*, $F_i^*(0) = \bar{f}_j$, $F_i^*(1) = f_i^*$.
(3) For each $i = 1, \ldots, n$, compute the shooting vector $v_i = \frac{\partial}{\partial t} F_i^*|_{t=0}$.
(3) Compute the average direction $\bar{v} = (1/n) \sum_{i=1}^{n} v_i$.
(3) If $\|\bar{v}\| < \varepsilon_1$, stop. Else, update using $\bar{f}_{j+1} = \bar{f}_j + \varepsilon_2 \bar{v}$.
(4) Set $j = j + 1$ and return to Step 1.

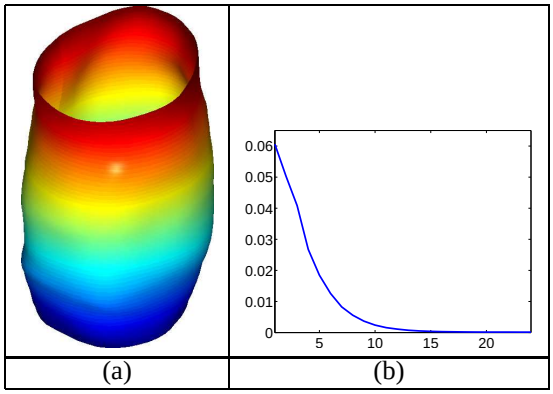

Figure 3: (a) Karcher mean of the given endometrial tissue surfaces. (b) Evolution of the energy gradient with iterations on the x-axis and gradient on the y-axis.

In Figure 3 we present the result of applying Algorithm 1 on our data set. In panel (a) we display the Karcher mean and in panel (b) we show the evolution of the gradient $\|\bar{v}\|$. The algorithm converged in approximately 25 iterations. Also, the computed mean is a nice representative of our data. The observed endometrial tissue surfaces are all cylindrical with local convex and concave structures. The Karcher mean is of similar structure.

3.2 Estimation of the Karcher Covariance

Once the sample Karcher mean has been computed, the evaluation of the Karcher covariance is performed as follows. The Karcher covariance captures the observed variability around the Karcher mean. First, we optimally register all surfaces in the sample to the Karcher mean $\bar{f}$, resulting in $\{f_1^*, \ldots, f_n^*\}$. Next, we find the shooting vectors from the mean $\bar{f}$ to each of the registered surfaces. That is, let $v_i = \frac{\partial}{\partial t} F_i^*|_{t=0}$, where $F_i^*(0) = \bar{f}$ and $F_i^*(1) = f_i^*$, $i = 1, 2, \ldots, n$. We then perform principal component analysis by applying the Gram-Schmidt procedure (under the chosen metric $\langle\langle \cdot, \cdot \rangle\rangle$), to generate an orthonormal basis $\{B_j | j = 1, \ldots, k\}$, $k \leq n$, of the observed $\{v_i\}$ in the vector space $T_{\bar{f}}(\mathcal{F})$. We project each of the vectors v_i onto this orthonormal basis using $v_i \approx \sum_{j=1}^{k} c_{i,j} B_j$, where $c_{i,j} = \langle\langle v_i, B_j \rangle\rangle_{\bar{f}}$. Now, each original surface can simply be represented using the coefficient vector $c_i = \{c_{i,j}\}$. Then, the covariance matrix can be computed in the coefficient space using $K = (1/(n-1)) \sum_{i=1}^{n} c_i c_i^T \in \mathbb{R}^{k \times k}$. We can use the SVD of K to determine the principal directions of variation in the given data. For example, if $u \in \mathbb{R}^k$ corresponds to a principal singular vector of K, then the corresponding tangent vector in $T_{\bar{f}}(\mathcal{F})$ is given by $\sum_{j=1}^{k} u_j B_j$. One can then map this vector to a surface $\bar{f}$ using the exponential map. We note that the exponential map is difficult to compute under the non-standard metric introduced earlier. Thus, we use a linear approximation. This approximation is reasonable in a neighborhood of the Karcher mean.

In Figure 4 we display the path traced by following the three main directions of variation from -1 standard deviation (blue) to $+1$ standard deviation (red) around the Karcher mean (green). These paths provide a natural set of representative deformations present in our data. Furthermore, they provide an efficient summary of the observed variability. Figure 5 provides a different visualization of the principal directions of variation. The first row provides the deformation vector field on the mean surface corresponding to each positive principal direction. The second row is a visualization of the point-wise magnitude of this vector field. This allows for easy identification of areas undergoing highest amounts of deformation.

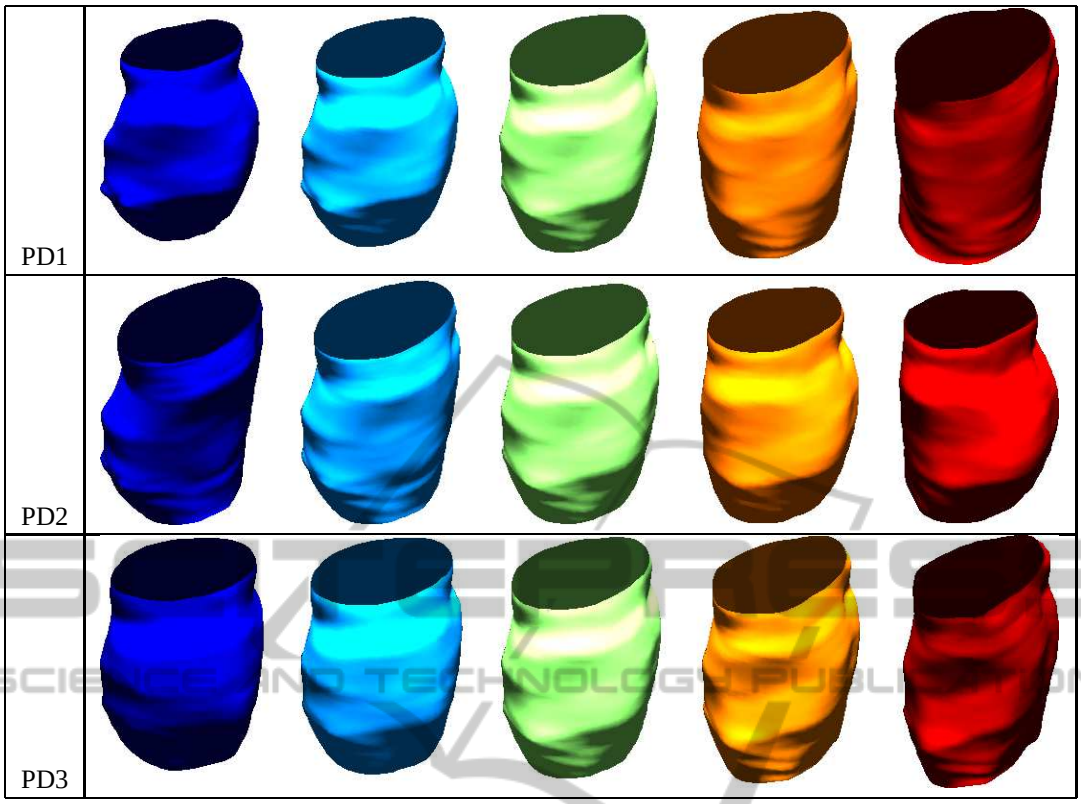

Figure 4: Three main directions of variation in the given data displayed as a path from -1 standard deviation (blue) to $+1$ standard deviation (red) around the Karcher mean (green).

3.3 Approximate Random Samples from Gaussian Model

Next, we validate our model using random sampling. For this purpose, we will utilize the Gaussian distribution defined in the tangent space at the mean endometrial tissue surface. A random tangent vector $v \in T_{\bar{f}}(\mathcal{F})$ can be generated using $v = \sum_{j=1}^{k} z_j \sqrt{S_{jj}} u_j B_j$, where $z_j \overset{iid}{\sim} N(0,1)$, S_{jj} is the variance of the jth principal component, u_j is the corresponding principal singular vector and B_j is a basis element. One can then obtain an approximate sample from the Gaussian distribution using a linear mapping $f = \bar{f} + v$.

In Figure 6, we show four randomly generated endometrial tissue surfaces using our approximate Gaussian model. A major motivation for random sampling in this application is that there are only few real data observations available. Thus, any analysis that requires many data observations will have to utilize simulation, which in turn requires a technique for random sampling. Note that, visually, all of the random samples generated using the described methodology are faithful representations of the given data, and thus, would be useful instances in any simulation study.

3.4 Summary

Statistical analysis of shapes of anatomical structures plays a key role for the validation of medical imaging techniques when monitoring and diagnosing complex diseases. We have presented a comprehensive framework for computing shape models of endometrial tissue surfaces. This framework, based on the square root normal field representation of cylindrical surfaces, enables one to register, compare, average and model endometrial tissue shapes. It also allows one to generate unobserved, random instances, which are useful for realistic simulations, especially when there is not enough real data for the validation process or it is biased. The resulting statistical models represent natural variability in observed data, and can be used by medical practitioners to characterize the variability in anatomical structure of the endometrial tissues.

A future direction of research is to validate the proposed statistical models of endometrial tissues by relating the generated random samples to a score provided by a medical expert. Our current claim is that

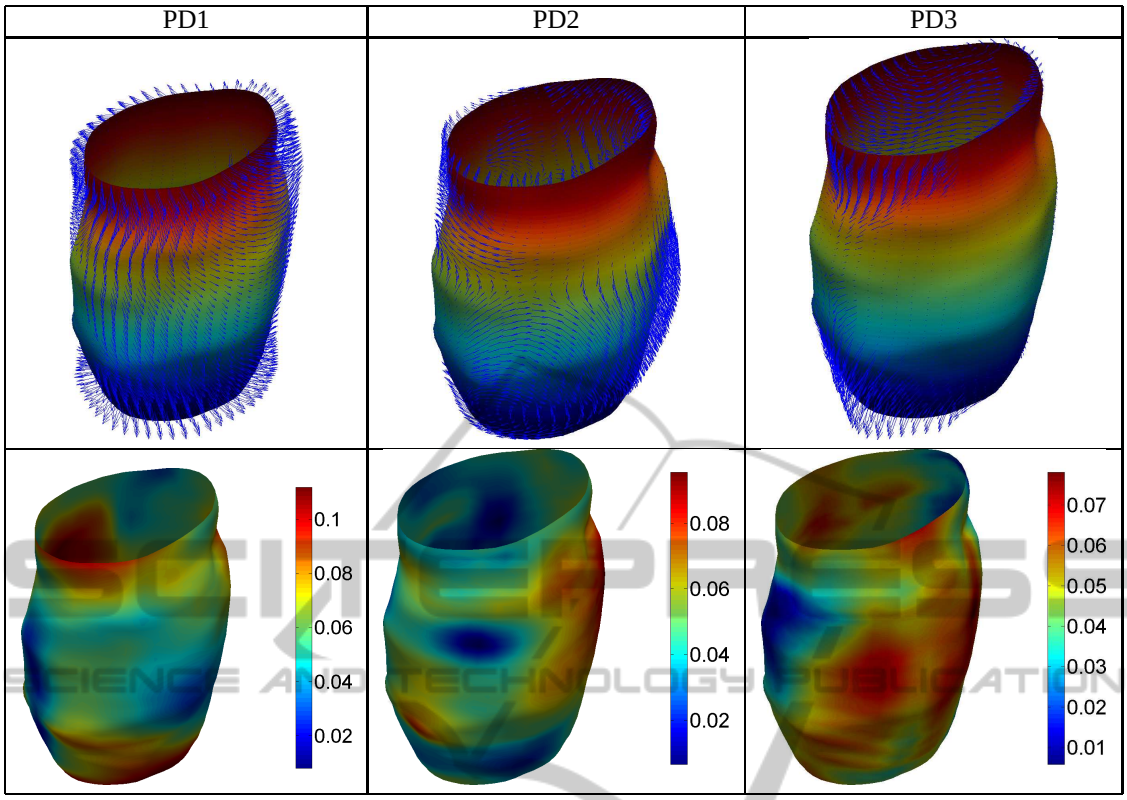

Figure 5: Principal direction deformation vector fields (top row) and their corresponding point-wise magnitudes (bottom row).

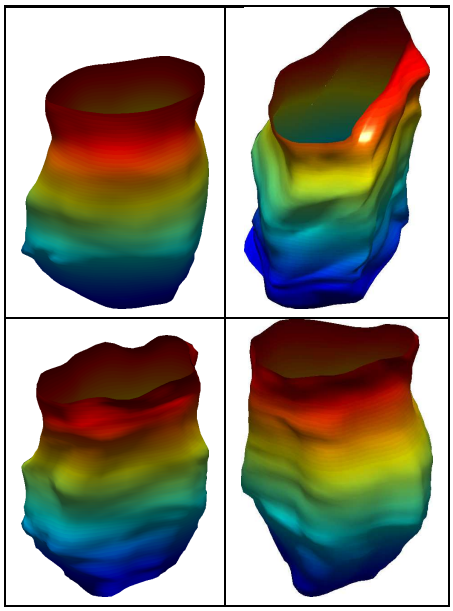

Figure 6: Four random endometrial tissue surfaces drawn from an approximate Gaussian model.

the generated samples visually resemble natural endometrial tissue surfaces. Adding a qualitative assessment from a medical expert would further support these claims. Another direction of future work can be the evaluation of registration and classification methods using the generated random samples.

REFERENCES

Almhdie, A., Léger, C., Deriche, M., and Lédée, R. (2007). 3D registration using a new implementation of the ICP algorithm based on a comprehensive lookup matrix: Application to medical imaging. *Pattern Recognition Letters*, 28(12):1523–1533.

Bouix, S., Pruessner, J. C., Collins, D. L., and Siddiqi, K. (2001). Hippocampal shape analysis using medial surfaces. *NEUROIMAGE*, 25:1077–1089.

Brechbühler, C., Gerig, G., and Kübler, O. (1995). Parameterization of closed surfaces for 3D shape description. *Computer Vision and Image Understanding*, 61(2):154–170.

Brosens, I., Puttemans, P., Campo, R., Gordts, S., and Kinkel, K. (2004). Diagnosis of endometriosis: pelvic endoscopy and imaging techniques. *Best Practice and Research Clinical Obstetrics and Gynaecology*, 18:285–303.

Cates, J., Meyer, M., Fletcher, P., and Whitaker, R. (2006). Entropy-based particle systems for shape correspondence. In *Proc. MICCAI Mathematical Foundations of Computational Anatomy*, pages 90–99.

Davies, R., Twining, C., Cootes, T., and Taylor, C. (2010). Building 3-d statistical shape models by direct optimization. *IEEE Trans. Medical Imaging*, 29(4):961–981.

Dryden, I. L. and Mardia, K. (1998). *Statistical Shape Analysis*. John Wiley & Son.

Gorczowski, K., Styner, M., Jeong, J., Marron, J., Piven, J., Hazlett, H., Pizer, S., and Gerig, G. (2010). Multi-object analysis of volume, pose, and shape using statistical discrimination. *IEEE Trans. Pattern Analysis and Machine Intelligence*, 32(4):652–666.

Grenander, U. and Miller, M. I. (1998). Computational anatomy: An emerging discipline. *Quarterly of Applied Mathematics*, LVI(4):617–694.

Gu, X., Wang, S., Kim, J., Zeng, Y., Wang, Y., Qin, H., and Samaras, D. (2007). Ricci flow for 3D shape analysis. In *Proc. IEEE International Conference on Computer Vision*.

Jermyn, I., Kurtek, S., Klassen, E., and Srivastava, A. (2012). Elastic shape matching of parameterized surfaces using square root normal fields. In *European Conference on Computer Vision*, pages 804–817.

Joshi, S., Miller, M., and Grenander, U. (1997). On the geometry and shape of brain sub-manifolds. *Pattern Recognition and Artificial Intelligence*, 11:1317–1343.

Kurtek, S., Klassen, E., Ding, Z., Avison, M., and Srivastava, A. (2011a). Parameterization-invariant shape statistics and probabilistic classification of anatomical surfaces. In *Proc. Information Processing in Medical Imaging*.

Kurtek, S., Klassen, E., Ding, Z., Jacobson, S., Jacobson, J., Avison, M., and Srivastava, A. (2011b). Parameterization-invariant shape comparisons of anatomical surfaces. *IEEE Trans. Medical Imaging*, 30(3):849–858.

Kurtek, S., Klassen, E., Ding, Z., and Srivastava, A. (2010). A novel Riemannian framework for shape analysis of 3D objects. In *Proc. IEEE Computer Vision and Pattern Recognition*, pages 1625–1632.

Kurtek, S., Klassen, E., Gore, J., Ding, Z., and Srivastava, A. (2012). Elastic geodesic paths in shape space of parametrized surfaces. *IEEE Trans. Pattern Analysis and Machine Intelligence*, 34(9):1717–1730.

Malladi, R., Sethian, J., and Vemuri, B. (1996). A fast level set based algorithm for topology-independent shape modeling. *Journal of Mathematical Imaging and Vision*, 6:269–290.

Styner, M., Oguz, I., Xu, S., Brechbuhler, C., Pantazis, D., Levitt, J., Shenton, M., and Gerig, G. (2006). Framework for the statistical shape analysis of brain structures using SPHARM-PDM. In *Proc. MICCAI Open Science Workshop*.

Yavariabdi, A., Samir, C., Bartoli, A., Ines, D., and Bourdel, N. (2013). Contour-based TVUS-MR image registration for mapping small endometrial implants. In *Abdominal Imaging. Computation and Clinical Applications*, volume 8198 of *Lecture Notes in Computer Science*, pages 145–154.